INTERNATIONAL SOCIETY FOR SOIL MECHANICS AND GEOTECHNICAL ENGINEERING

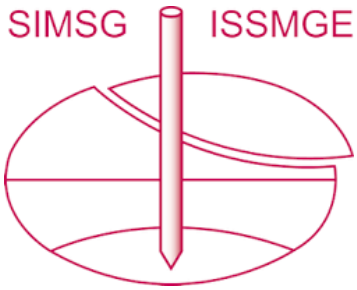

This paper was downloaded from the Online Library of the International Society for Soil Mechanics and Geotechnical Engineering (ISSMGE). The library is available here:

https://www.issmge.org/publications/online-library

This is an open-access database that archives thousands of papers published under the Auspices of the ISSMGE and maintained by the Innovation and Development Committee of ISSMGE.

The paper was published in the Proceedings of the 8th International Symposium on Deformation Characteristics of Geomaterials (IS-PORTO 2023) and was edited by António Viana da Fonseca and Cristiana Ferreira. The symposium was held from the 3rd to the 6th of September 2023 in Porto, Portugal.

IS-PORTO 2023 PROCEEDINGS

Proceedings of the 8th International Symposium on
DEFORMATION CHARACTERISTICS OF GEOMATERIALS
Porto, 3rd - 6th September 2023

Isotropic compression simulation of kaolinite using coarse-grained molecular dynamics

Yohei Nakamichi[1#], *Catherine* O'Sullivan[1], *Stefano* Angioletti-Uberti[2], *Paul* Tangney[2,3], and *Sara* Bandera[4]

[1]*Imperial College London, Department of Civil and Environmental Engineering, SW72AZ London, UK*
[2]*Imperial College London, Department of Materials, SW72AZ London, UK*
[3]*Imperial College London, Department of Physics, SW72AZ London, UK*
[4]*University of Pavia, Department of Civil Engineering and Architecture (DICAr), Via Ferrata, 3, 27100, Pavia, Italy*
[#]*Corresponding author: yohei.nakamichi21@imperial.ac.uk*

ABSTRACT

It is now viable to use coarse-grained molecular dynamics (CGMD) to model interacting clay particles in simulations of soil mechanics element tests. In CGMD, particle interactions are described by the Gay-Berne (GB) potential, which can approximate the potential energy between clay particles as a function of their separation and relative orientations; however, a previous study identified a significant shortcoming of the GB potential, which is that it lacks a local maximum called the "energy barrier" that the true interaction possesses at very close range. In this study, we propose a modified GB potential which can capture the energy barrier at and we use this new potential function to simulate the clay mineral kaolinite under isotropic compression. Our simulations show that the energy barrier is a crucial ingredient required to reproduce the elastoplastic behaviour observed in laboratory tests upon unloading from an isotropic normally consolidated state. Our data show that the difference in mechanical behaviour between normally consolidated clay and overconsolidated clay can be explained by the fact that, during the initial loading, some pairs of interacting particles surmount the energy barrier so that they then experience a large attractive force. Effectively, these particles become bounded and do not separate when the stress applied to the sample is released. The response of overconsolidated clay to applied stress is stiffer than that of normally consolidated clay because a larger proportion of the clay particle interactions exist in this bonded state.

Keywords: coarse-grained molecular dynamics; kaolinite; isotropic compression; Gay-Berne potential.

1. Introduction

The behaviour of clay is quite complex. When compared to that of other types of soil, such as gravel, sand and silt, its compressibility is high, its volumetric change upon mechanical loading is significant, and its shear strength is low. Clay shows time-dependent deformation due to the slow dissipation of excess pore water pressures during consolidation, which leads to significant challenges in construction projects.

Lambe and Whitman (1969) highlighted that the mechanical behaviour of clay is highly affected by its microstructure. From a geotechnical engineering perspective, the microstructure of clay is defined as the combination of the interactions between particles and the microfabric (Mitchell and Soga, 2005). It is generally known that the microstructure of clay is influenced by the electro-chemical characteristics of the surfaces of clay particles; however, because clay particles are very fine, it is difficult to investigate the behaviour of individual clay particles experimentally or to study how the microstructure at the particle-scale influences the mechanical behaviour at the engineering scale.

Particle-scale simulations, in which detailed data on individual particles and particle interactions can be obtained, are the most effective tools to investigate this fundamental issue. In geotechnical engineering, the discrete element method (DEM) is well-established as a useful research tool, but it has mainly been applied to particle-scale simulations of sand or gravel. There are few examples of its use for particle-scale simulations of clay.

Recently, coarse-grained molecular dynamics (CGMD) has been applied in particle-scale simulations of clay. The validity and the effectiveness of CGMD were firstly shown by Ebrahimi et al. (2014), who used CGMD to simulate the behaviour of Na-montmorillonite during isotropic compression. Later, Bandera et al. (2021) used CGMD to simulate kaolinite particles. In both studies, clay particles were modelled as plate-like rigid ellipsoids. In CGMD, the interaction between two particles is described by an interparticle potential, which is the potential energy of interaction between them, as a function of their separation (h). The earlier research studies indicated that interactions between two clay particles modelled by rigid ellipsoids can be reasonably described by the Gay-Berne (GB) potential (Gay and Berne, 1981), which is a variation of the Lennard-Jones potential. Although it has been proposed that CGMD can be used to simulate both Na-montmorillonite and kaolinite, CGMD is fundamentally better suited to simulate kaolinite because kaolinite particles are generally more rigid and have a flatter, more plate-like morphology than montmorillonite particles (Bandera, 2021).

The GB potential parameters do not have an obvious physical meaning and must be calibrated by comparison with existing data and/or theoretical models (Ebrahimi et al., 2014). For example, Bandera et al. (2021) used DLVO theory (Derjaguin and Landau, 1941; Verwey and Overbeek, 1948), named after Derjaguin-Landau-Verwey-Overbeek, to calibrate their GB model parameters; DLVO theory was originally proposed to describe interactions between colloidal particles in a suspension. Ebrahimi et al. (2014) conducted fully atomistic molecular dynamics simulations of Na-montmorillonite particles, and calibrated their GB potential parameters for use in CGMD simulations based on the data from these atomistic simulations.

Bandera et al. (2021) identified some limitations of using CGMD with the GB potential to simulate assemblies of kaolinite particles. One important issue is that the GB potential cannot reproduce the local maximum called the "energy barrier" in the potential energy that exists at a short separation (h_{eb}). It seems plausible that this energy barrier may influence the loading and unloading behaviours of clay during consolidation. However, the influence of the energy barrier on the mechanical behaviour of clay is not well established.

This work explores how the energy barrier influences the mechanical behaviour of kaolinite within CGMD framework used by Bandera et al. (2021). We begin by outlining how DLVO theory can be used to calibrate the GB potential for describing the interaction between two kaolinite particles. Then we propose a modified GB potential, which possesses the energy barrier at short particle-particle separations. We use the modified GB potential in CGMD simulations of isotropic compression of kaolinite to investigate how the response of kaolinite is modified by the energy barrier.

1.1. Net force and potential energy between particles

Fig. 1(a) and 1(b) illustrate how the net force between two kaolinite particles and their potential energy of interaction, respectively, depend on their surface-to-surface distance (h). At long distances, the force is repulsive, but at very short distances, it becomes attractive. The energy barrier in Fig. 1(b) is located at h_{eb}, this is a point where the force in Fig. 1(a) changes from being repulsive to attractive as the particles approach one another. At a shorter separation distance ($h = h_{\mathrm{ew}}$), there is a local minimum in the interaction potential energy at the bottom of a deep "energy well". There is also a much shallower local minimum at long distances ($h \gg h_{\mathrm{eb}}$), but when we use the term "energy well", we are referring to the deeper energy well at shorter separations.

As shown in Fig. 1(b), if a pair of particles are forced together, such that their separation distance reduces from $h > h_{\mathrm{eb}}$ to $h < h_{\mathrm{eb}}$, they enter the energy well and their interaction energy lowers dramatically. This means that an even larger energy barrier, which is also at h_{eb}, but when approached from the other side, must be surmounted to separate them again. In other words, when two particles are bound together by pushing them together, it requires more energy (a greater average force) to pull them apart again.

The net force between particles can be divided into two components, i.e. a mechanical (contact) force and an electrical (non-contact) force (Mitchell and Soga, 2005). The distinction between mechanical and electrical force is somewhat arbitrary, as in essence they are both manifestations of the electrostatic forces present between electrons and nuclei. However, whereas the mechanical force is quantum mechanical in nature, electrical force is typically described within the realm of classical electrostatics. More precisely, the mechanical (contact) force is a very short-range repulsion that manifests itself when the surface-to-surface distance is less than the distance at which the minimum of the energy well exists ($h < h_{\mathrm{ew}}$). This force finds its origins in Pauli's exclusion principle for electrons but is typically referred to as Born's repulsion. In essence, as two clay particles get closer to each other, the outer electron shells of atoms of the clay surface start to overlap. Pauli's exclusion principle dictates that this must lead to an increase in the electron's kinetic energy, and this increase in energy manifests in an overall effective repulsion between nuclei. Born's repulsion increases steeply as the surface-to-surface distance decreases and prevents excess particle overlap and particle penetration.

At separation distances that exceed the energy well ($h > h_{\mathrm{ew}}$), the electrical (non-contact) force is dominant. It is generally recognized that the electrical (non-contact) force is the balance between the van der Waals attraction and the double layer repulsion. As two clay particles get closer to each other, both the van der Waals attraction and the double layer repulsion increase. However, at short surface-to-surface distances (over the interval between the energy well and the energy barrier, i.e. $h_{\mathrm{ew}} < h < h_{\mathrm{eb}}$), the net force is attractive because the van der Waals attraction is stronger than the double layer repulsion. On

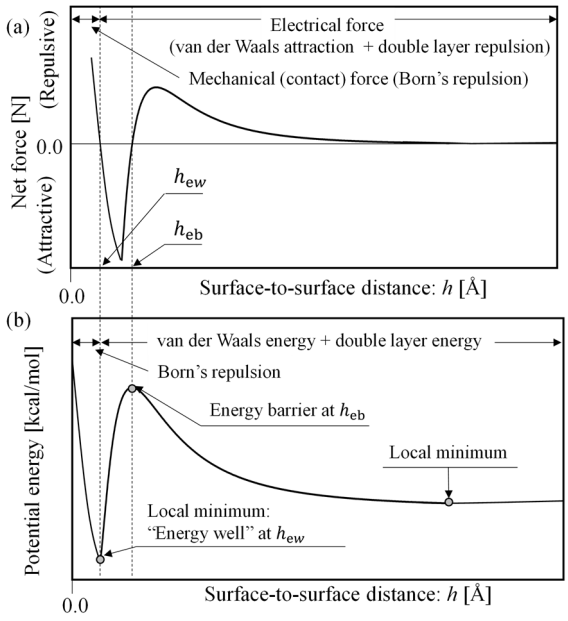

Figure 1. Schematic interaction between two kaolinite particles (a) relationship between net force and surface-to-surface distance (b) relationship between potential energy and surface-to-surface distance adopted by Lu et al. (2008)

the other hand, as the surface-to-surface distances increase and beyond the energy barrier ($h > h_{eb}$), the opposite occurs and the net force becomes repulsive.

The energy barrier and the energy well define a range of separation distances over which the interaction force is attractive because the net force is the negative slope of the potential energy - surface-to-surface distance relationship. Hence, it can be speculated that the heights and positions of the energy barrier and the energy well have an impact on the mechanical behaviour of kaolinite.

The height and position of the energy barrier are influenced by the salt concentration and the pH of the liquid surrounding the particles. For example, Gupta (2011) showed that the silica face-to-alumina face interaction of kaolinite has a high energy barrier in an alkaline solution (e.g. pH = 8) while it does not have any energy barriers at all in an acidic solution (e.g. pH = 4). Gupta (2011) also showed that the surface charge decreases with an increasing salt concentration in an alkaline (e.g. pH = 8) solution, which implies that the energy barrier is lower at higher salt concentrations. This effect should be expected as it is a simple manifestation of screening effects due to mobile salt ions. It generally decreases the strength of monopole-monopole electrostatic interactions, decreasing the contribution of the double-layer repulsion, and thus the height of the energy barrier decreases.

1.2. DLVO theory

In geotechnical engineering, it is assumed that interactions between clay particles can be calculated based on DLVO theory. DLVO theory describes the relationship between potential energy and separation distance of two parallel semi-infinite plates. Although DLVO theory can also predict the potential energy acting on finite bodies (e.g. spheres and ellipsoids) by using the Derjaguin approximation (Israelachvili, 2011), its implementation is not trivial. Hence, this study assumes two kaolinite particles in a face-to-face configuration interact as two parallel semi-infinite plates, i.e. the shape of the clay particle is not considered.

In DLVO theory, the potential energy is given by the sum of the van der Waals energy and the double layer energy via the following equation:

$$E_T = E_{vdw} + E_{Edl} \quad (1)$$

where E_T is the total energy of interaction per unit area, E_{vdw} is van der Waals energy per unit area and E_{Edl} is the double layer energy per unit area.

The van der Waals energy per unit area, E_{vdw} [kcal/mol/Å^2], can be described by:

$$E_{vdw} = -\frac{A_H}{12\pi}\left[\frac{1}{h^2} + \frac{1}{(h+\delta_1+\delta_2)^2} - \frac{1}{(h+\delta_1)^2} - \frac{1}{(h+\delta_2)^2}\right] \quad (2)$$

where A_H [kcal/mol] is the Hamaker constant, h [Å] is the separation distance between the two surfaces, and δ_1 [Å] and δ_2 [Å] are the thicknesses of the two plates, and Å (angstrom) is the unit of length (1 Å = 10^{-10} m).

The double layer energy per unit area, E_{Edl} [kcal/mol/Å^2], is given by:

$$E_{Edl} = \varepsilon_r \epsilon_0 \kappa \left[\frac{2\psi_1\psi_2 e^{\kappa h} - \psi_1^2 - \psi_2^2}{e^{2\kappa h} - 1}\right] \times 1.4393 \times 10^4 \quad (3)$$

where ψ_1 [mV] and ψ_2 [mV] are the surface potentials of the two plates, ε_r [-] is the relative permittivity, ϵ_0 [F/m] is the permittivity of free space and κ [Å^{-1}] is the thickness of the double layer.

Mitchell and Soga (2005) detailed the fundamental structure of a kaolinite particle. Fig. 2 gives the schematic view of a structure of a kaolinite particle. A kaolinite particle consists of a silica sheet, which has a tetrahedral silicate unit structure, and an alumina sheet, which has an octahedral alumina unit structure. Gupta (2011) investigated the electrochemical characteristics of the kaolinite particle surface and showed that the three faces of a kaolinite particle, i.e. the silica face, the alumina face, and the edge have different charges that depend upon the pH and salt concentration of the electrolyte solution surrounding the clay platelets. Gupta (2011) calculated the DLVO parameters for the representative particle configurations shown in Fig. 3, i.e. the face-to-face configuration (silica face-to-alumina face configuration) and the edge-to-edge configuration.

Table 1 shows the DLVO parameters for a particle saturated in an electrolyte with a 1 mM salt concentration and a pH of 8, calculated by Gupta (2011). Fig. 4 shows the relationships between the potential energy and the surface-to-surface distance for the face-to-face configuration and the edge-to-edge configuration calculated using these parameters. As shown in Fig. 4, as the two particles approach each other at very short separation distances, the potential energy decreases because Born's repulsion is not considered in DLVO theory.

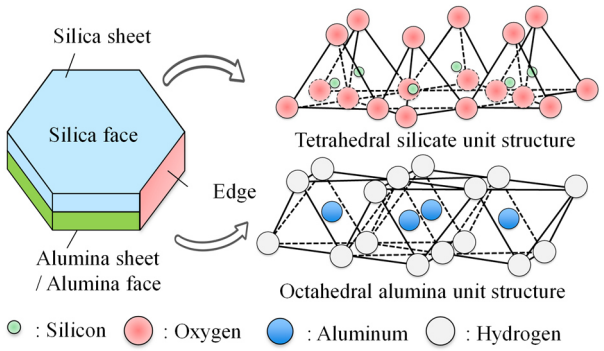

Figure 2. Schematic diagrams of structure of kaolinite particle

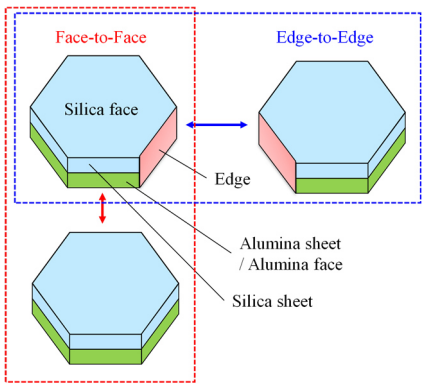

Figure 3. Representative particle configurations: Face-to-Face and Edge-to-Edge

Table 1. DLVO parameters of kaolinite saturated in an electrolyte solution in salt concentration 1mM at pH 8

DLVO parameter	Face-to-Face	Edge-to-Edge
A_H [kcal/mol]	2.994	3.411
$\delta_1 = \delta_2$ [Å]	2,000.0	20,000.0
ε_r [-]	78.0	78.0
ϵ_0 [F/m]	8.854×10^{-12}	8.854×10^{-12}
$1/\kappa$ [Å]	96.0	96.0
ψ_1 [mV]	-67.05	-219.97
ψ_2 [mV]	-55.27	-219.97

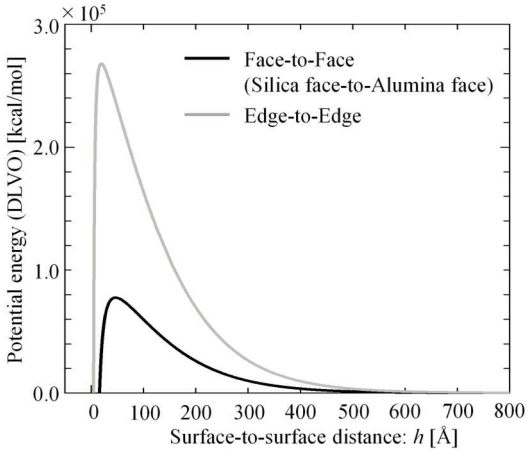

Figure 4. Relationship between potential energy and surface-to-surface distance calculated by DLVO theory

1.3. Gay-Berne potential

The GB potential is an anisotropic potential function developed from the Lennard-Jones potential explicitly for ellipsoidal particles. The GB potential is given by the following equation:

$$GB^{12-6} = 4\varepsilon\left[\left(\frac{\sigma}{h_{12}+\gamma\sigma}\right)^{12} - \left(\frac{\sigma}{h_{12}+\gamma\sigma}\right)^{6}\right] \times \eta \times \chi \qquad (4)$$

where ε [kcal/mol] is the energy scale, σ [Å] is the atomic interaction radius, h_{12} [Å] is the closest distance between particles which is related to particle size and orientation, and γ [-] is the shift of the potential minimum. The dimensionless quantities, η [-] and χ [-] are the shape anisotropy and the energy anisotropy, respectively. χ is calculated considering the three energy anisotropic parameters, ε_a[-], ε_b [-] and ε_c [-].

Amongst these parameters, only h_{12} and η can be explicitly determined from particle shape, position, and orientation. The other GB potential parameters do not have clear physical meanings, and cannot be directly determined from the properties of kaolinite particles; these are tunable parameters that must be calibrated. Bandera et al. (2021) calibrated the tunable GB potential parameters to fit the relationships between the potential energy and separation distance for the face-to-face and the edge-to-edge configurations calculated by using DLVO theory. This is based on the fact that, at least qualitatively, if the face-to-face and edge-to-edge configurations can be calibrated correctly, the GB functional form can correctly extrapolate the value of the potential energy for intermediate orientations, at least for particles of ellipsoidal symmetry (Gay and Berne, 1981).

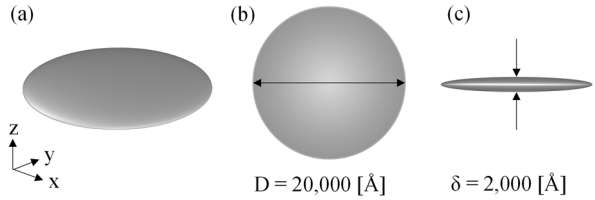

Figure 5. Rigid Ellipsoidal model of kaolinite (a) overhead view (b) plane view (diameter) (c) side view (thickness)

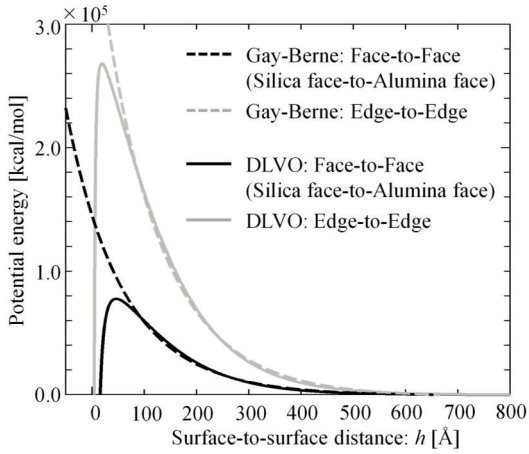

Figure 6. Calibration results of the Gay-Berne potential against DLVO theory

The current study calibrated the GB parameters by using DLVO theory, following Bandera et al. (2021). Fig. 5 shows the rigid ellipsoid model of the kaolinite particle used in the calibration of the GB^{12-6} potential (Eq. (4)). The size of this rigid ellipsoid model was determined by referring to Bandera et al. (2021). Fig. 6 shows the results of the calibration for the face-to-face and the edge-to-edge configurations, respectively. Although the GB^{12-6} potential accurately captures DLVO theory from medium separation distances to long separation distances, it cannot reproduce the reduction of the potential energy at short separation distances. In other words, this potential function cannot reproduce the energy barrier and the energy well.

2. Modified Gay-Berne potential

As outlined in the previous section, the most critical limitation of the GB^{12-6} potential is that it cannot reproduce the energy barrier and the energy well that exist at short separation distances. Hence, the influence of the energy barrier and of the energy well on the mechanical behaviour of kaolinite cannot be addressed using particle-scale simulations with this description. In this study, to model the energy barrier and the energy well, a new potential function was developed by modifying the GB^{12-6} potential. The modified GB potential function is given by:

$$aGB^{12-24} = 4\varepsilon\left[\left(\frac{\sigma}{h_{12}+\gamma\sigma}\right)^{12} - \left(\frac{\sigma}{h_{12}+\gamma\sigma}\right)^{24} + Ce^{-h_{12}/\sigma_0}\right] \times \eta \times \chi \quad (5)$$

where C [-] and σ_0 [-] are the new fitting parameters. The aGB$^{12\text{-}24}$ potential has two repulsive components and one attractive component, specifically, the first term: $(\sigma/(h_{12}+\gamma\sigma))^{12}$ and the third term: Ce^{-h_{12}/σ_0} are repulsive, while the second term: $(\sigma/(h_{12}+\gamma\sigma))^{24}$ is attractive.

The exponent of the attractive term in the aGB$^{12\text{-}24}$ potential is 24 while it is 6 in the GB$^{12\text{-}6}$ potential. The exponent of the repulsive term is 12 in both the GB$^{12\text{-}6}$ potential and the aGB$^{12\text{-}24}$ potential. The main reason why 24 and 12 were used as exponents for the attractive term and repulsive term respectively in the aGB$^{12\text{-}24}$ potential is that mathematically the exponent of the attractive term needs to be larger than the repulsive term to reproduce the local maximum (the energy barrier). The value of 24 has no specific physical meaning; rather, 24 was chosen for the exponent of the attractive term in the aGB$^{12\text{-}24}$ potential because it is twice the value of the exponent of the repulsive term.

The second repulsive term: Ce^{-h_{12}/σ_0} is used to model the mechanical (contact) force, which is shown in Fig 1 (a) and (b). The purpose of this repulsive term is to avoid excessive overlapping of particles and particle interpenetration. It is necessary to calibrate the newly introduced fitting parameters, C and σ_0, so that when the separation distance between two particles approaches zero, it rapidly produces a large repulsive force, which at the same time makes the energy well.

Fig. 7 compares the shapes of the GB$^{12\text{-}6}$ and the aGB$^{12\text{-}24}$ potential functions. As shown in Fig. 7(a), in the GB$^{12\text{-}6}$ potential, where the exponent of the attractive term is smaller than that of the repulsive term, only a local minimum develops at short separation distances. On the other hand, as shown in Fig. 7(b), in the aGB$^{12\text{-}24}$ potential, where the exponent of the attractive term is larger than that of the repulsive term and the term modelling mechanical (contact) force is added, both the local maximum (energy barrier) and the local minimum (energy well) at short separation distances are captured.

The GB$^{12\text{-}6}$ potential is then only suitable to describe the interactions at separation distances greater than the separation distance at which the energy barrier exists, i.e. $h > h_{\text{eb}}$. A modification of the GB$^{12\text{-}6}$ potential was suggested by Bandera et al. (2021), as shown in Eq. (6). This modified potential considered only the repulsive term of the GB$^{12\text{-}6}$ potential with the aim of reproducing the purely repulsive energy-separation distance profile at $h > h_{\text{eb}}$ as predicted by DLVO theory for kaolinite saturated at an alkaline pH.

$$GB^{12-} = 4\varepsilon\left[\left(\frac{\sigma}{h_{12}+\gamma\sigma}\right)^{12}\right] \times \eta \times \chi \quad (6)$$

Bandera et al. (2021) indicated that applying Eq. (6) does not present a problem during a loading simulation of kaolinite. However, the applicability of the GB$^{12\text{-}}$ to an unloading simulation has not yet been investigated. Here, we hypothesise that when the target loading pressure is above a critical threshold, the particle separation distance will fall below h_{eb} (see Fig. 1) and particles will be attracted to each other, which we expect to change their behaviour during unloading.

In this study, parameters for both the aGB$^{12\text{-}24}$ and GB$^{12\text{-}}$ potentials were calibrated against DLVO theory, following Bandera et al. (2021). The calibrations were

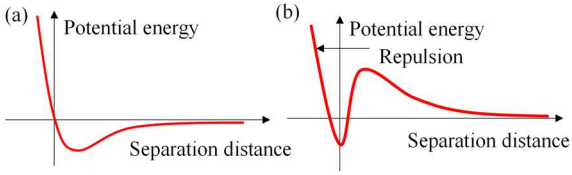

Figure 7. Shape of Gay-Berne potential (a) GB$^{12\text{-}6}$ potential (b) aGB$^{12\text{-}24}$ potential

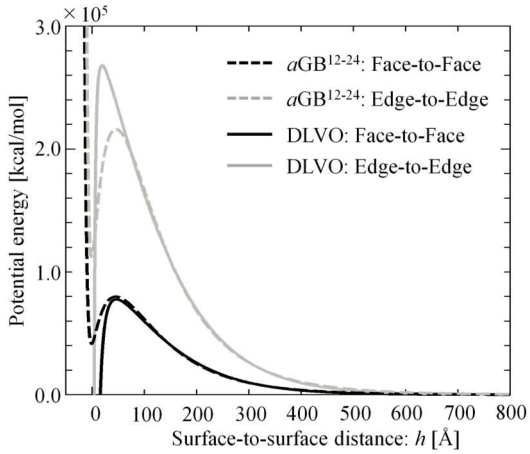

Figure 8. Calibration result of aGB$^{12\text{-}24}$ potential

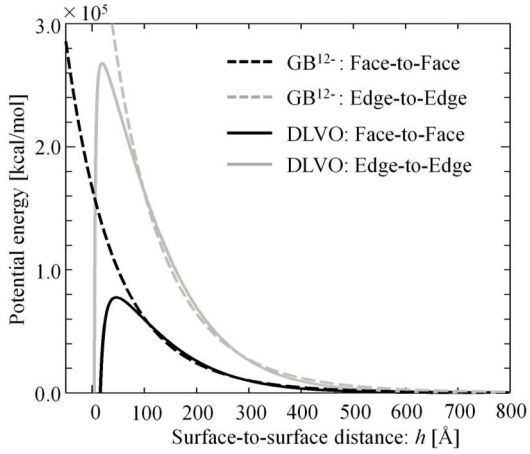

Figure 9. Calibration result of GB$^{12\text{-}}$ potential

Table 2. Gay-Berne potential parameters for aGB$^{12\text{-}24}$ potential and GB$^{12\text{-}}$ potential

GB parameter	aGB$^{12\text{-}24}$ potential	GB$^{12\text{-}}$ potential
γ [-]	1.01	0.57
ε [kcal/mol]	67.2	0.43
σ [Å]	923.7	1996.0
ε_a [-] = ε_b [-]	636.8	63.5
ε_c [-]	235.0	23.7
C [-]	8.0	—
σ_0 [-]	4.0	—

conducted using the DLVO parameters shown in Table 1. In both cases, the kaolinite particles were modelled as the rigid ellipsoids shown in Fig. 5. Fig. 8 and 9 show the calibration results for the aGB$^{12\text{-}24}$ potential and the GB$^{12\text{-}}$ potential, respectively, and Table 2 shows their calibrated GB parameters. In the calibration of the aGB$^{12\text{-}24}$ potential, as DLVO theory cannot describe the mechanical (contact) force, the parameters of the repulsion term newly introduced to model the mechanical (contact) force were determined so that the energy well appears at zero separation distance ($h = 0$). The GB$^{12\text{-}}$ potential was calibrated against DLVO theory for the separation distances longer than the separation distance at which the energy barrier appears ($h > h_{\mathrm{eb}}$).

3. Isotropic compression simulation

3.1. Simulation conditions

In this study, isotropic compression simulations using CGMD framework were carried out using the MD code LAMMPS (Plimpton, 1995) to investigate the influence of the energy barrier and the energy well on the isotropic compression behaviour of kaolinite. Two scenarios were considered: in the first one, both the energy barrier and the energy well were considered (aGB$^{12\text{-}24}$ potential), while in the second one, the energy barrier and the energy well were not considered (GB$^{12\text{-}}$ potential). The parameters for the calibrated potential functions used in these simulations are presented in Table 2.

The virtual CGMD simulation sample used for the isotropic compression simulation is shown in Fig. 10(a) and comprises 1,000 particles. Bandera et al (2021) outlined that a system with only 1,000 particles is too small to generate meaningful data for fabric analysis, however, this sample size is sufficient for the current proof-of-concept study. All 1,000 particles in the simulation sample had the same size (diameter: 20,000 Å, thickness: 2,000 Å, aspect ratio: 10), in other words, we study a mono-disperse sample. As an initial arrangement of particles, 10 particles were placed equally spaced along the x, y and z axes, and each particle was given a random orientation. The initial spacing between the centres of the particles was 20,500 Å, which is larger than the particle diameter (20,000 Å), to avoid initial overlapping of the particles. The velocity of each particle was assigned based on the gaussian distribution of kinetic energies with temperature at 300 K. As shown in Fig. 10(b), periodic boundary conditions were imposed to reproduce a bulk material behaviour using a small sample size. For simplicity, the effects of gravity and other external forces imparted during soil deposition process were ignored. The particle surfaces were assumed to be sufficiently smooth, i.e. contact friction between particles was not considered in the simulations. The pore fluid is implicit, in other words, the water chemistry is accounted for in the DLVO expressions, and it is assumed that the compression is so slow that no excess pore water pressure is generated, i.e. it is a fully drained simulation.

Fig. 11 shows the simulation workflow adopted from Bandera et al (2021). Before performing the isotropic compression simulations, a sample equilibration phase was conducted to equilibrate the system. In the sample equilibration phase, a NVE simulation was first performed to check the energy conservation of the system and to find a suitable simulation time-step. In the NVE simulation, the number of particles (N), volume (V) and energy (E) of the system remain constant. As a second step in the sample equilibration phase, a NVT simulation, was performed. In the NVT simulation, the number of particles and the volume are kept constant during the simulation, and the temperature (T) of the system can be controlled to simulate thermal equilibrium. In this study, the NVT simulation was performed at 300 K. After the NVT simulation, a NVE simulation was performed again to check the equilibration state and the energy conservation.

Table 3 summarises the isotropic compression simulation conditions. The same simulation conditions were used for both scenarios: when modelling the energy barrier and the energy well (aGB$^{12\text{-}24}$ potential), and when omitting the energy barrier and the energy well (GB$^{12\text{-}}$ potential). A small time-step was used to meet the critical time-step requirement for numerical stability. The loading speed was determined with reference to Bandera et al (2021) so that the deformation of the simulation sample was quasi-static. Initial loading and unloading simulations were conducted to study the behaviour of the simulation sample. The unloading simulation was

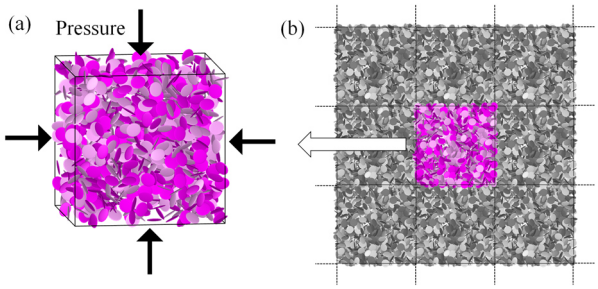

Figure 10. Simulation sample (a) overhead view of simulation sample (b) image of periodic boundary condition

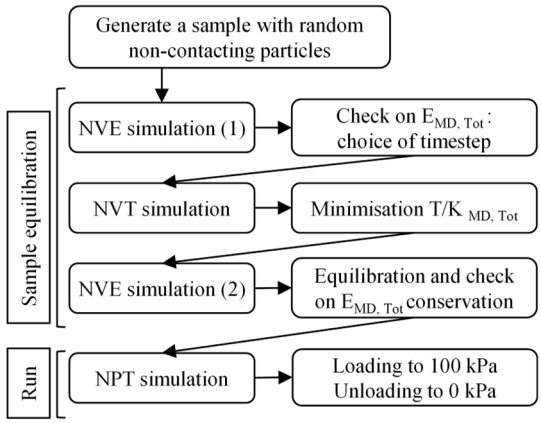

Figure 11. Workflow of isotropic compression simulation

Table 3. Isotropic compression simulation conditions

Number of particles	1000 [-]
Time-step	1.0×10^{-11} [s]
Total simulation time	1.0×10^{-2} [s]
Loading speed	2.0×10^{4} [kPa/s]
Pressure	0.0→100.0→0.0 [kPa]

performed immediately after completing the initial loading simulation. The maximum isotropic pressure was set to be 100 kPa. The isotropic pressure was linearly increased from 0 kPa to 100 kPa in the initial loading phase and was linearly decreased from 100 kPa to 0 kPa in the unloading phase.

3.2. Results

Fig. 12 shows the relationship between the void ratio and the isotropic pressure for both scenarios. When the GB^{12-} potential is used (the energy barrier and the energy well are not modelled), the response of the simulation sample during the unloading phase is overall stiffer than the response observed during the initial loading phase. This response is similar to that observed in laboratory tests for normally consolidated and overconsolidated kaolinite specimens. Hence, these data suggest that this potential function at least partially captures the fundamental elastoplastic behaviour of kaolinite. However, if we go more into detail, the initial loading curve and the unloading curve follow the same path in the pressure interval P = 45-100 kPa. This suggests that the simulation sample exhibits reversible and elastic behaviour at this pressure level (P=45-100 kPa). This response does not reflect the physical reality, where a stiffer response is expected from the onset of unloading.

On the other hand, when the $a GB^{12-24}$ potential is used (the energy barrier and the energy well are modelled, unlike the GB^{12-} potential we just discussed), the initial loading curve and the unloading curve are not collinear at any pressure level. These data indicate that the simulation sample exhibits irreversible behaviour even in the pressure interval P = 45-100 kPa.

The only difference between the two scenarios is the type of potential function employed. Therefore, we deduce that modelling the energy barrier and the energy well is essential to simulate the irreversible behaviour of kaolinite under isotropic compression at all pressures, with particular reference to the differences in stiffness during normal consolidation and unloading.

To further understand the origin of the different behaviours observed, we study the configuration of the particles obtained during the simulations. Fig. 13 shows the relationship between face-to-face coordination number and isotropic pressure for both scenarios. The face-to-face coordination number indicates how many particle pairs are in face-to-face contact, normalized by the total number of particles. The face-to-face coordination number was calculated from the particle positions and orientations following the protocol described by Ebrahimi et al. (2014).

In the sample simulated with the GB^{12-} potential, thus omitting the energy barrier and the energy well, as shown in Fig. 13(a), the face-to-face coordination number and the isotropic pressure are in a one-to-one relationship; during the initial loading phase, as the pressure increases, the particle contacts increase, whereas during the unloading phase, the particles move away from each other as the pressure decreases. When the energy barrier and the energy well are modelled using the $a GB^{12-24}$ potential, the situation is radically different, as shown in Fig. 13(b). Whereas the behaviour during the loading phase is similar to that with the GB^{12-} potential, upon unloading the face-to-face coordination number does not decrease at all and remains constant. This suggests that the particles that came together during initial loading do not separate from each other and maintain contact during the unloading phase. This behaviour occurs because many interparticle interactions are pushed into the energy well during the initial loading phase and remain stuck there even during unloading because the energy barrier is too large to overcome, generating an irreversible behaviour. Capturing the energy barrier in the use of the $a GB^{12-24}$ potential function results in a collective particle behaviour that exhibits irreversible volume change. Thus, we conclude that the energy barrier is a key feature of particle interactions that contributes to the difference

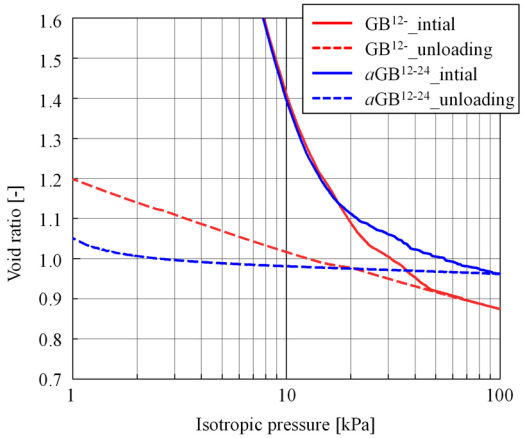

Figure 12. Relationship between void ration and isotropic pressure

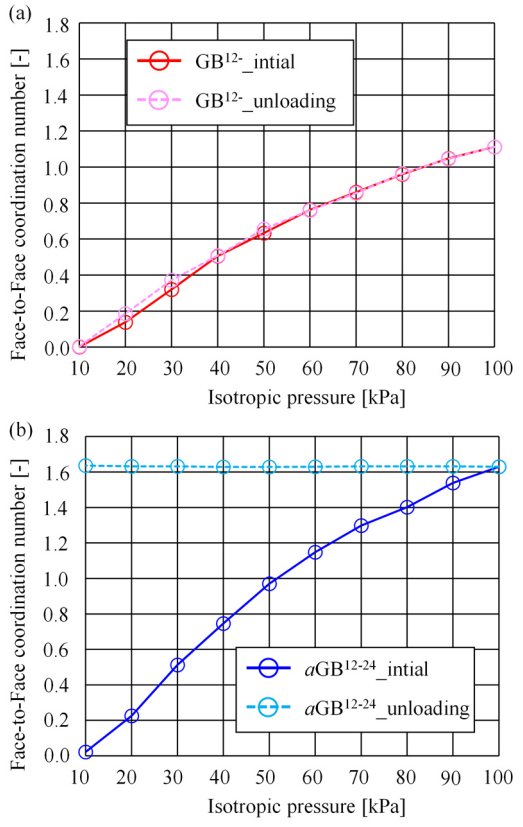

Figure 13. Face-to-face coordination number in (a) GB^{12-} potential (b) $a GB^{12-24}$ potential

between normally consolidated and overconsolidated kaolinite behaviours.

4. Conclusions

We have proposed a new potential function, aGB$^{12\text{-}24}$, developed to simulate the interaction of kaolinite particles in coarse-grained molecular dynamics (CGMD) simulations. This new potential function is a modified version of the Gay-Berne (GB) potential that can reproduce the energy barrier and the energy well existing at short separation distances in the potential energy-separation distance profiles, describing the interaction between two kaolinite particles. Isotropic compression simulations of kaolinite were performed using two modified GB potentials (the aGB$^{12\text{-}24}$ potential and the GB$^{12\text{-}}$ potential) to investigate the effects of the non-monotonic nature of the potential function relating to the interaction energy and the particle separation on the mechanical behavior of kaolinite.

The GB$^{12\text{-}}$ potential does not model the energy barrier nor the energy well that exists in the relationship between the potential energy and separation distance between particles. In the new aGB$^{12\text{-}24}$ potential formulation, the energy barrier was modelled by making the exponent of the attraction term larger than the exponent of the repulsion term. The energy well was modelled in this study by introducing a strongly repulsive mechanical contact force, which exists at a short separation distance.

The results from isotropic compression simulations using the aGB$^{12\text{-}24}$ potential and the GB$^{12\text{-}}$ potential showed that the energy barrier and energy well play an important role in the mechanical behaviour of clay. In the scenario omitting the energy barrier and energy well (GB$^{12\text{-}}$ potential), our simulations showed a reversible and elastic behaviour in the pressure interval 45-100 kPa, while in the scenario modelling the energy barrier and energy well (modelled using the aGB$^{12\text{-}24}$ potential), the system showed the typical irreversibility observed in real kaolinite samples. From these results, it was confirmed that the presence of the energy barrier and energy well contribute to the difference in mechanical response between normally and overconsolidated clays.

While in the scenario omitting the energy barrier and energy well (GB$^{12\text{-}}$ potential), the face-to-face coordination number decreased with decreasing pressure during the unloading phase, in the scenario modelling the energy barrier and the energy well (aGB$^{12\text{-}24}$ potential), the face-to-face coordination in the unloading phase did not decrease from the initial loading phase even though the pressure applied on the simulation sample decreased. In other words, the difference in mechanical response between normally- and over- consolidated clays is caused by the fact that many interparticle interactions are pushed out into the energy well during the initial loading, but during unloading, the interparticle interactions cannot overcome the energy barrier and are confined in the energy well.

For reasons of computational efficiency, this study used the small sample size (1,000 particles) for the isotropic compression simulations. However, the sample size used in this study is not sufficient to generate meaningful data for fabric analysis (Bandera et al., 2021). Hence, these data are preliminary in nature, and we need to use a larger sample size (e.g. 10,000 particles) to develop more definitive conclusions.

We must acknowledge also that the model considered here includes significant simplifications. The limitations of DLVO theory, on which the interaction model is based are outlined in Mitchell and Soga (2005). The way the samples are made differs from the sedimentation of in situ clay deposits. The uniform particle sizes, uniformity of the assumed surface charge, are additional limitations of the model.

Acknowledgements

The first author is supported by OBAYASHI Corporation and Imperial College Dixon Scholarship. Sara Bandera's doctoral research was funded by the Leverhulme Trust, (Project no. RPG-2017-055). Simulations were carried out using the High-Performance Computer (HPC) facilities at Imperial College London and University College London. We are grateful to the UK Materials and Molecular Modelling Hub for computational resources, which is partially funded by EPSRC (EP/P020194/1 and EP/T022213/1).

References

Bandera, S., O'Sullivan, C., Tangney, P., Angioletti-Uberti, S. 2021. "Coarse-grained molecular dynamics simulations of clay compression", Comput Geotech, Volume 138. https://doi.org/10.1016/j.compgeo.2021.104333

Derjaguin, B., Landau, L.D. 1941. "Theory of the stability of strongly charged lyophobic sols and of the adhesion of strongly charged particles in solution of electrolytes", Acta Physicochimica U.R.S.S. 14, pp. 633-662.

Ebrahimi, D., Whittle, A. J., Pellenq, R. J. M. 2014. "Mesoscale properties of clay aggregates from potential of mean force representation of interactions between nanoplatelets", J Chem Phys, Volume 140, Issue 15. https://doi.org/10.1063/1.4870932

Gay, J. G., Berne, B. J. 1981. " Modification of the overlap potential to mimic a linear site-site potential", J Chem Phys, volume 74, pp. 3316-3319. https://doi.org/10.1063/1.4870932

Gupta, V. 2011. "Surface Charge Features of Kaolinite Particles and Their Interactions", PhD thesis, The University of Uhta.

Israelachvili, J. N. 2011. "Intermolecular and Surface Forces", 3rd ed., Academic Press, Massachusetts, US. https://doi.org/10.1016/C2009-0-21560-1

Lambe, T.W., Whitman, R. V. 1969. "Soil Mechanics". John Wiley & Sons, New York, US.

Lu, N., Anderson, M. T., Likos, W. J., Mustoe, G. W. 2008. "discrete element model for kaolinite aggregate formation during sedimentation", Int J Numer Anal Methods Geomech, Volume 32, pp. 965-980. https://doi.org/10.1002/nag.656

Mitchell, J. K., Soga, K. 2005. "Fundamentals of soil behavior", 3rd ed., John Wiley & Sons, New Jerjey, US.

Plimpton, S.J. 1995. "Short-Range Molecular Dynamics". J Comput Phys, Volume 117, Issu 1, pp. 1–19. https://doi.org/10.1006/jcph.1995.1039

Verwey, E. J. W., Overbeek, J. Th. G. 1948. "Theory of the Stability of Lyophobic Colloids: The Interaction of Sol Particles Having an Electric Double Layer", Elsevier, Amsterdam, Netherland.